

# The use of satellite NDVI data for the validation of global vegetation phenology models: application to the Frankfurt Biosphere Model

Matthias K.B. Lüdeke<sup>a,\*</sup>, Peter H. Ramage<sup>b</sup>, G.H. Kohlmaier<sup>b</sup>

<sup>a</sup> Potsdam Institute for Climate Impact Research, Telegrafenberg C4, Postfach 60 12 03, 14412 Potsdam, Germany

<sup>b</sup> Institute for Physical and Theoretical Chemistry, Johann Wolfgang Goethe-University, D-60439 Frankfurt, Germany

Received 14 December 1994; accepted 10 October 1995

---

## Abstract

An algorithm based on a three-spline function fitted to measured NDVI courses (normalized difference vegetation index) was developed to analyze a given NDVI annual course with respect to leaf shooting and leaf abscission times of deciduous vegetation. In contrast to algorithms which are based on modified second derivatives of the NDVI time course to detect shooting or abscission, the proposed algorithm takes into account the whole annual time course and is therefore less sensitive to noise in the NDVI-signal. In the present study this algorithm was used to validate the phenology results for the deciduous vegetation of a global equilibrium run of the prognostic Frankfurt Biosphere Model (FBM, spatial resolution  $0.5^\circ \times 0.5^\circ$ ) driven by a climatology which represents a mean seasonality of the driving variables. The mean value of the area-weighted frequency distribution of the difference between the shooting date deduced from NDVI and the shooting date calculated by the FBM for the deciduous vegetation types is  $-4$  days, indicating that in the global mean the FBM predicts leaf shooting less than one week too late. A 75% fraction of the area under consideration shows predicted shooting dates lying within a range of  $\pm 30$  days compared to the satellite-derived dates. The distribution has its maximum at a difference of 0 days (i.e. the FBM exactly fits the NDVI deduced shooting day for these areas). This result supports the general assumption that at least in global scale models phenology can be successfully deduced from carbon flux balance considerations.

*Keywords:* Phenology; Normalized difference vegetation index; Vegetation dynamics; Leaf shooting; Leaf abscission

---

## 1. Introduction

From the beginning of the 1980s, NOAA (National Oceanic and Atmospheric Administration) constructed global maps of the NDVI (normalized difference vegetation index) using data measured by an AVHRR (advanced very high resolution radiometer) on board the NOAA satellites. The AVHRR instrument globally measures the reflectance  $a_i$  in different channels 'i', i.e. the ratio between incident and reflected solar radiation

---

\* Corresponding author. Fax: (49) (331) 288-2600; e-mail: luedeke@pik-potsdam.de

by the Earth's surface in different wavelength bands. The NDVI is defined as the following combination of the near infrared ( $i = N$ ,  $\lambda$ : 725–1100 nm) and the visible red ( $i = R$ ,  $\lambda$ : 580–680 nm) channel:

$$\text{NDVI} = \frac{a_N - a_R}{a_N + a_R} \quad (1)$$

At about 700 nm plants show a pronounced jump in reflectance caused by the weak reflectance of chlorophyll and other leaf pigments in the visible wave band ( $a_R$ ) versus the strong reflection of leaves in the near infrared band ( $a_N$ ). In contrast, bare soil is characterized by a slight monotonous increase in reflectance with wavelength, while the reflectance of water surfaces even decreases with wavelength for a fixed solar zenith angle. From these properties follows that the NDVI defined according to Eq. 1 shows high values up to 1 for areas covered with dense green vegetation ( $a_N \rightarrow 1$ ,  $a_R \rightarrow 0$ ) and small values for bare soil ( $a_N \approx a_R$ ). In the case of water surfaces the NDVI may even drop to negative values.

Attempts were made to evaluate time series of the global NDVI in order to determine the carbon uptake fluxes of the vegetation (Ruimy et al., 1991; Sellers et al., 1992), the leaf area index (Tucker and Sellers, 1986; Lüdeke et al., 1991) as well as the vegetation types present (Tucker et al., 1985). In this study, we use NDVI time series (NGDC, 1992) for the determination of the foliation period of deciduous vegetation which seems to be a more direct interpretation of the vegetation index. Nevertheless we had to establish an appropriate algorithm to calculate the shooting date and the date of total discoloration from a given NDVI time series. In the following section, we present a new three-spline algorithm which yields reasonable results even for noisy NDVI signals as the comparison with ground observations at various phenological gardens shows.

In another section we compare the phenological data derived from the NDVI time courses with the shooting and total discoloration dates as predicted by the Frankfurt Biosphere Model (FBM). The FBM is a global model for calculating the seasonal pattern of uptake and release of  $\text{CO}_2$  by vegetation and soil in a steady state climate simulation as well as the long-term development in a changing environment (Janecek et al., 1989; Kindermann et al., 1993; Lüdeke et al., 1994, 1995). In contrast to other global vegetation models (e.g. the TEM, Raich et al., 1991) there is no separate and specifically parameterized phenology module, but leaf shooting and abscission is triggered by the carbon flux balance of the vegetation in the sense that leaf abscission starts when the carbon balance becomes negative (respirational 'costs' exceed assimilation 'gains') while leaf shooting starts when the carbon balance is positive after conversion of the stored assimilates into leaves. Therefore phenology validation in the case of the FBM is a test of the whole model performance. In Appendix A we present a short summary of the main model characteristics. A detailed description of the FBM is given in Lüdeke et al. (1994).

In Fig. 1 we display the deciduous vegetation types considered in the FBM and their respective total areas. Since in the FBM calculations the *potential* vegetation is considered, we had to exclude from the comparison those areas with strongly different actual vegetation. Furthermore areas with unreliable NDVI data, e.g. as caused by water surface effects, were omitted (for details see Section 3).

## 2. Detecting shooting and abscission dates from the NDVI-signal

To analyze a given annual course of NDVI with respect to leaf shooting and leaf abscission times of areas predominantly vegetated with deciduous plants we developed an algorithm based on a three-spline function which is fitted to the measured NDVI courses.

The three splines represent the phenophases of leaf shooting (A:  $t \in [t_1; t_2]$ ), a phase of constant and then decreasing LAI (B:  $t \in [t_2; t_3]$ ) followed by the phase of dormancy (C:  $t \in [t_3; t_1]$ ). Inspection of measured NDVI courses of deciduous vegetation sites suggested a linearly increasing function for phase A, a decreasing parabolic function for phase B starting with slope 0 and a  $x$ -axiparallel straight line for the dormancy phase (C).

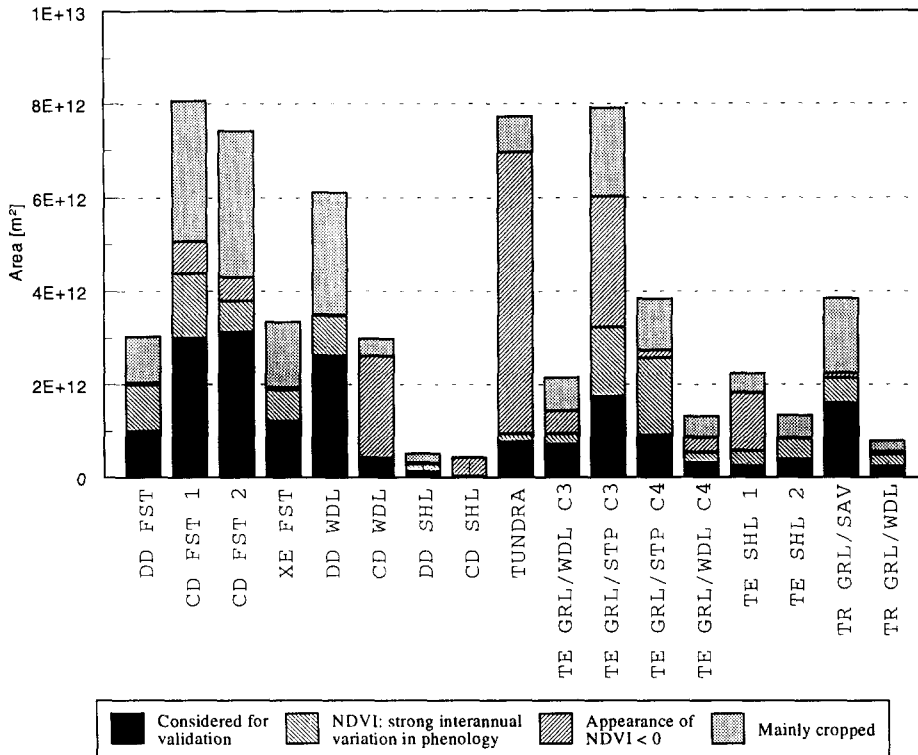


Fig. 1. Bars: areas of potential deciduous vegetation (Matthews, 1983) considered in the FBM calculations. Black segments: areas remaining for phenology validation after singling out areas of strongly different actual vegetation or unreliable NDVI data (for details see Section 3, for abbreviations see Appendix D).

For the explicit parametrization of the spline-function and the details of the numerical fitting procedure see Appendix B. In Fig. 2 two monthly NDVI courses (a: Southeast Quebec, cold deciduous forests with evergreens, and b: (near) Caracas, Venezuela, drought deciduous woodland, both 1986) together with their spline fits are shown. As an appropriate measure of the quality of the fit we used the mean absolute error divided by the annual NDVI amplitude. For the two cases displayed the relative error amounts to 0.07 and 0.13, respectively. These examples characterize the error range of all grid elements considered for validation (95% of the grid elements range between 0.6 and 0.15 with an average of 0.11).

In contrast to algorithms which are based on modified second derivatives of the NDVI time courses to identify shooting or abscission times, the proposed algorithm takes into account the whole annual time course and is therefore less sensitive against situations where there is considerable noise in the NDVI-signal.

To calibrate the spline-algorithm we compared the phenology of *cold deciduous tree species* as observed at different European phenological gardens (Schnelle, 1985) and phenological observations in the USA compiled by Schwartz and Marotz (1986) with our evaluation of the corresponding NDVI courses. For every phenological garden assumed to be characteristic for each region, we used the monthly NDVI courses of the years 1986, 1987 and 1988 (spatial resolution 10' × 10') and determined the averages of  $t_1$  and  $t_2$ . As shown in Fig. 3a, all observed mean shooting dates (averages over the observed woody species and over the time period of 1973–1982 (Europe) and 1961–1980 (USA), respectively) lie within phase A, which stands for the period of

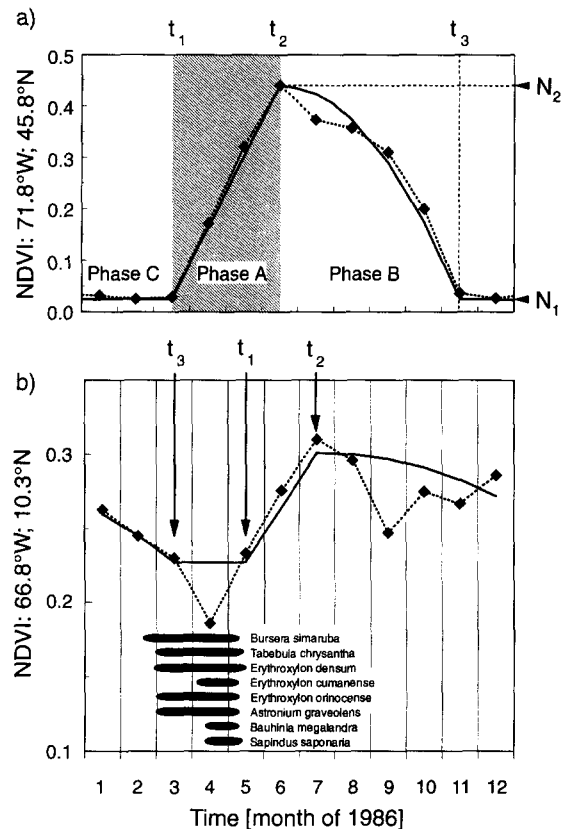


Fig. 2. Two monthly NDVI courses for 1986 (rhombi with dashed lines) together with their spline fits (solid lines, see text). (a) Shaded area: phase of mainly increasing NDVI, defined by the  $[t_1, t_2]$  time interval (phase A). Southeast Quebec, cold deciduous forest with evergreens. (b) Horizontal bars: leafless periods of different drought deciduous woody perennials as observed at the Botanical Garden of Caracas in 1986.

mainly increasing NDVI. We define the relative position  $r_t$  of the shooting date within  $[t_1, t_2]$ -interval as follows:

$$r_t = \frac{t - t_1}{t_2 - t_1} \quad (2)$$

Mean leaf shooting of the observed species of the considered ecosystem type occurs on average after a fraction of  $r_t = 0.4$  of the  $[t_1, t_2]$ -interval has passed. This delay (compared with  $t_1$ ) is due to earlier leaf shooting dates of the herbaceous vegetation detected by the satellite, too.

In a phenological study of the tree, shrub and herb layer of oak/beech forests in Germany (Ellenberg, 1982), the shooting dates of the herbaceous plants were observed about the middle of February, the shrubs started to unfold their leaves at about the end of March while the average shooting date of the trees was the end of April. The canopies of the trees were fully developed about the end of May. Therefore the time period between the first leaf emergence and this date ( $\Delta t_{\text{obs}}$ ) was about 3.5 months which is in good agreement with the average of the  $[t_1, t_2]$ -intervals obtained from the NDVI courses of the 16 regions investigated amounting to 3 months and 25 days. Furthermore the observed first shooting dates for the woody plants are at about the end of March. This is a delay of a fraction of 0.43 of the  $\Delta t_{\text{obs}}$  time period with respect to the date of first leaf emergence and

therefore agrees with the mean behaviour of the calibration sites considered, with an average value of  $r_i = 0.4$  (standard deviation  $\sigma = 0.13$ ).

For the remaining deciduous vegetation types the small number of available phenological observations necessitated performing several isolated tests of the proposed procedure for NDVI interpretation:

- For the *drought deciduous woody vegetation type* the phenological observations of Olivares and Medina (1992) at the Botanical Garden of Caracas in 1986 allows for a comparison with the evaluation of the corresponding NDVI course for 1986, as shown in Fig. 2b. Although the NDVI signal appears to be rather noisy the proposed evaluation algorithm detects the period of dormancy (the  $[t_3, t_1]$  interval) in keeping with the observed leafless periods of the species considered. A detailed phenological spectrum of a drought deciduous woodland in southern Zaire (27.3°E, 11.3°S) for the years 1971 and 1972 was set up by Malaisse (1974). Averaging of shooting and abscission dates of the 18 deciduous species considered in this study yielded a mean abscission date of day #172 and a mean shooting date of day #279. The NDVI courses for this location and the years 1986–1988 were evaluated. The resulting average  $t_3$  and  $t_1$  values (day #187 and day #269, respectively) are in good agreement with the observations, if one takes into account the interannual variability in start and end of the dry season triggering phenology.
- For the *drought deciduous shrubland* we performed a more qualitative comparison with the observations on shrubs in the Mojave Desert in 1971 (116.2°W, 36.8°N; Nevada, USA) published by Ackerman and Bamberg (1974). According to their investigation six dominant deciduous plant species constitute about 80% of the total plant cover in this area. The shooting period of a 75% fraction of this deciduous plant cover was observed to last from late January to early February (in the remaining areas it started at the end of March). In this region the event of leaf shooting is triggered by winter rains which are regular and wide spread. Therefore the observations can be regarded as typical and a comparison with the result of the NDVI evaluation is reasonable. Using the grid element (116.2°W, 36.8°N) for the three NDVI data sets on hand (1986–1988), we calculated an average  $t_1$  value of 25 (range: 15–45) which coincides with the observed leaf shooting and shows that even for small absolute NDVI-amplitudes (here: 0.02) the proposed algorithm yields reliable results.
- For the *steppe / prairie (C3)* vegetation type we compared the phenological description of a typical southern *Stipa* grassland of the western Eurasian steppe belt (Walter, 1968) with the NDVI-evaluation of a corresponding region (57.3°E, 47.8°N) actually covered with natural grasslands according to Olson and Watts (1982). Here we detected a shooting date  $t_1$  at day #91 which corresponds with the reported start of strong LAI-increase around 15 April. The mean detected  $t_2$  of day #137 fits the observed time of the maximum of vegetative development in mid May. The end of the vegetation period caused by drought is observed to be about mid July which equals the mean  $t_3$  value of #198.

From the above tests we conclude that the proposed algorithm allows for the determination of the shooting and abscission dates of various ecosystem types with reasonable accuracy even from noisy NDVI courses. Furthermore, it was possible to calibrate the algorithm for detecting the shooting times of the dominant woody species of cold deciduous forest ecosystems, which in general are delayed compared to the first leaf emergence of herbaceous understory vegetation.

### 3. Comparison of the global NDVI derived phenology with results of the Frankfurt Biosphere Model (FBM)

In this section we compare the shooting and abscission dates, as calculated in a global FBM equilibrium run, with the respective values derived from the NDVI observations for the years 1986–1988 according to the algorithm described in the previous section. We start with the cold deciduous forests where we could quantitatively test the performance of the NDVI evaluation algorithm against an appropriate number of ground data sets.

Therefore we first identified the  $0.5^\circ \times 0.5^\circ$  grid elements with potential cold deciduous or mixed forests according to Matthews (1983). We then omitted those which at present are mainly cropped according to Olson and Watts (1982) as well as those showing temporarily negative NDVI values, e.g. during snow melting, and therefore not interpretable on the basis of the spline algorithm presented here (this effect is explained in detail in Appendix C). We then evaluated the NDVI courses for the years 1986, 1987 and 1988 (NGDC, 1992) for the remaining 4201 grid elements constituting an area of  $8.2 \cdot 10^6$  km<sup>2</sup> to obtain three  $\{t_1, t_2, t_3\}$  sets for each grid element. For each grid element the three sets were averaged in order to derive a data set appropriate for the intended intercomparison with the FBM phenology calculations which were based on mean climatic variables. We then determined the standard deviation  $\sigma$  of the 3-year averages of the shooting time ( $t_1$ ) and excluded the grid elements with  $\sigma > 20$  days. This was done in order to avoid the comparison of vegetated regions showing a strong annual variability in phenology (e.g. caused by strongly varying weather conditions) with the corresponding FBM results which at present are not based on the actual annual weather courses of 1986–1988 but on a 30-year mean climate. Furthermore strong annual variability in the results of the evaluation algorithm could indicate occasionally occurring artefacts in the NDVI signal (e.g. long periods of dense cloud cover) which under certain circumstances would lead to an unrealistic mapping of the phenology. Phenological data of deciduous temperate forests in Germany and the Netherlands evaluated by Kramer (1994) indicate  $\sigma$  values of about 10 days, which is considerably lower than the chosen threshold of 20 days, i.e. grid elements with a typical annual variation in phenology are included in the comparison performed.

In a first comparison effort the mean  $t_1$  values of the remaining 3280 grid elements, which represent an area of  $6.1 \cdot 10^6$  km<sup>2</sup>, were compared with the FBM computed shooting time by calculating the relative position  $r_t$  of the respective day number within the  $[t_1, t_2]$  interval of the respective grid element (see Eq. 2). Fig. 3b shows the area-weighted frequency distribution, i.e. the area sums of grid elements within given  $r_t$ -intervals, which arose from this first comparison. The shaded area represents the time interval of mainly increasing NDVI. One would expect to find the FBM calculated shooting times for the dominant woody vegetation within this interval. Comparison of Fig. 3b with 3a, the latter described in the previous section, yields that the distribution of shooting dates calculated with the FBM (mean position:  $r_t = 0.30$ ;  $\sigma: 0.18$ ) is very similar to the distribution observed at the phenological gardens (mean position:  $r_t = 0.40$ ;  $\sigma: 0.13$ ). Thus the FBM phenology, based on

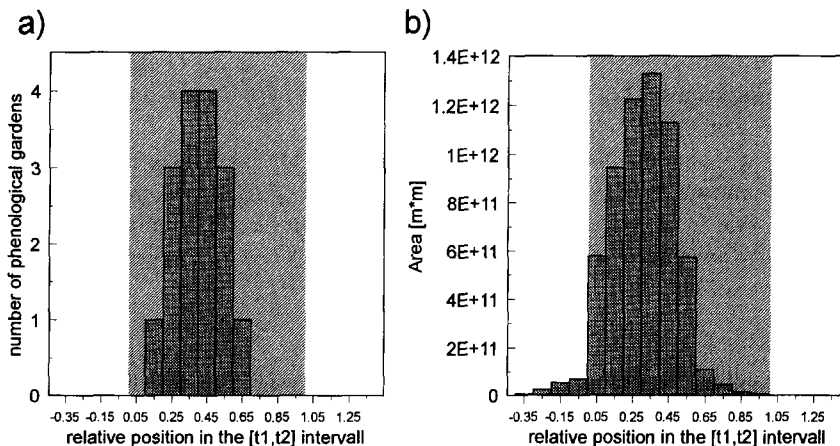


Fig. 3. (a) Frequency distribution of the relative position of the mean shooting dates for cold deciduous tree species as observed at 16 European phenological gardens (from  $47^\circ$  to  $59^\circ$  latitude, for details see text) with respect to the corresponding NDVI-derived  $[t_1, t_2]$  intervals. Shaded area: observation lies within the time interval of increasing NDVI. The average value is  $r_t = 0.40$  ( $\sigma = 0.13$ ). (b) Same plot as (a), showing the FBM-predicted shooting dates of actual cold deciduous and mixed forests (considered: 3280  $0.5^\circ \times 0.5^\circ$  grid elements with a total area of  $6.13 \cdot 10^{12}$  m<sup>2</sup>, see Fig. 1) in the  $[t_1, t_2]$  intervals. The average value is  $r_t = 0.30$  ( $\sigma = 0.18$ ). For details see Section 3.

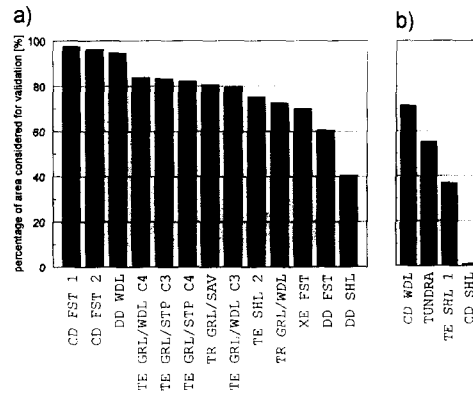


Fig. 4. Total area of grid elements where the FBM calculated shooting date lies within the  $[t_1, t_2]$  interval determined from the NDVI signal (i.e. the interval of mainly increasing NDVI) as a percentage of the area under consideration. (a) Vegetation types with NDVI < 0 values appearing in less than half the area of actual occurrence or (b) more than half the area. For the abbreviations of the vegetation type names see Appendix D.

the simulated carbon flux balance only, predicts the shooting times of the temperate woody vegetation reasonably well.

Fig. 4 shows the integrated results of the above analysis applied to all deciduous vegetation types. We calculated the total area of grid elements where the FBM predicted shooting date lies within the  $[t_1, t_2]$  interval determined from the NDVI signal (i.e. the interval of mainly increasing NDVI) as a percentage of the area considered (black bars in Fig. 1).

The bad agreement of the FBM-predictions with the NDVI-deduced shooting periods in e.g. the cold deciduous shrublands and the tundra ecosystems is probably caused by the delayed rise of the NDVI-signal due to simultaneous occurrence of melting snow and green vegetation in springtime, even in grid elements where the NDVI-value stays positive during the whole year. This effect is described in greater detail in Appendix B by tracing the NDVI courses of tundra grid elements along a north/south transect. Generalizing this argument we omitted the vegetation types from our analysis which show negative NDVI-values in more than half the area of their actual occurrence (displayed in Fig. 4b).

Inspection of Fig. 4a, displaying the results based on probably reliable NDVI evaluations, yields for seven vegetation types that for more than 80% of the considered area leaf shooting is predicted to lie within the time interval of mainly increasing NDVI which is a satisfactory correspondence of the FBM-calculations and the NDVI courses.

For the tropical/subtropical drought deciduous forests and the drought deciduous shrublands values less than 70% are found indicating either poor model performance of the FBM or a remarkable difference between the 1986–1988 climate and the 30-year average climate used to drive the FBM for the grid elements of these drought deciduous vegetation types.

In Fig. 5 the mean relative position of the shooting days calculated by the FBM within the  $[t_1, t_2]$  interval is depicted for the different vegetation types. Most of the mean  $r_t$ -values range from 0.10 to 0.45 while the two vegetation types which correlate rather weakly with the NDVI signal (DD FST and DD SHL) show smaller values. Neglecting these two vegetation types one obtains that the FBM predicts a mean  $r_t$ -value of 0.35 for vegetation types which are clearly dominated by woody species (CD FST 1 and 2; XE FST; DD WDL; TE SHL) being in accordance with the phenological observations for the cold deciduous forests ( $r_t = 0.40$ , Fig. 3a) while, as one would expect, the mean predicted shooting dates for the remaining herbaceous and mixed vegetation types are closer to  $t_1$  (mean  $r_t$ -value of about 0.20).

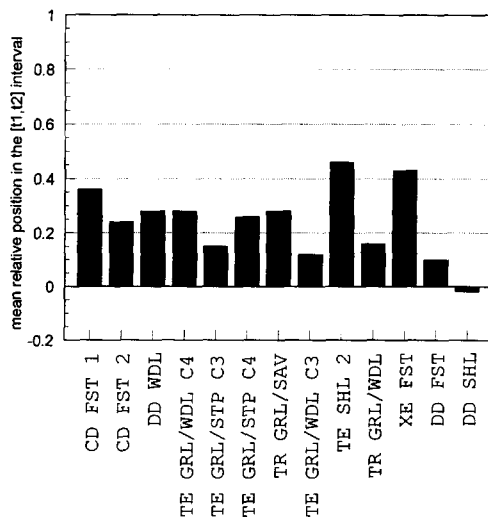


Fig. 5. Bars: mean relative position of the FBM-calculated shooting date within the NDVI-deduced  $[t_1, t_2]$  interval for the vegetation types listed in Fig. 4a.

To perform a more explicit comparison with respect to the shooting date we applied the  $r_t = 0.40$  value as determined in the previous section to all grid elements of the vegetation types CD FST, DD WDL, XE FST and DD FST which are dominated by woody species. For all remaining vegetation types the herbaceous species play a major role with regard to the carbon exchange fluxes and therefore are included in the FBM parametrization. In this case the FBM calculations should also reproduce the early leaf shooting of the herbaceous species. So here we applied a value of  $r_t = 0$  to calculate the shooting date from the respective NDVI courses.

The area-weighted frequency distribution of the difference of the NDVI-deduced shooting date and the FBM-calculated shooting date for all vegetation types listed in Fig. 4a is shown in Fig. 6. This distribution was obtained by calculating the error in every grid element, sorting the grid elements into error classes and finally adding up the grid element areas in every error class. The mean value of these differences (errors) is  $-4$  days,

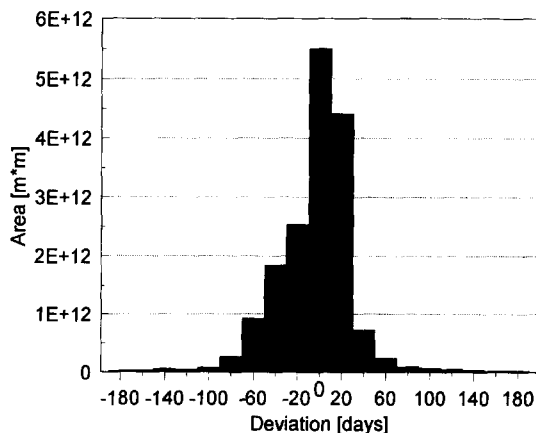


Fig. 6. Area-weighted frequency distribution of the deviation of the FBM-calculated shooting date from the NDVI-deduced shooting date for the vegetation types listed in Fig. 4a. Positive deviation values indicate that the FBM-calculated shooting date is earlier than the NDVI-deduced.

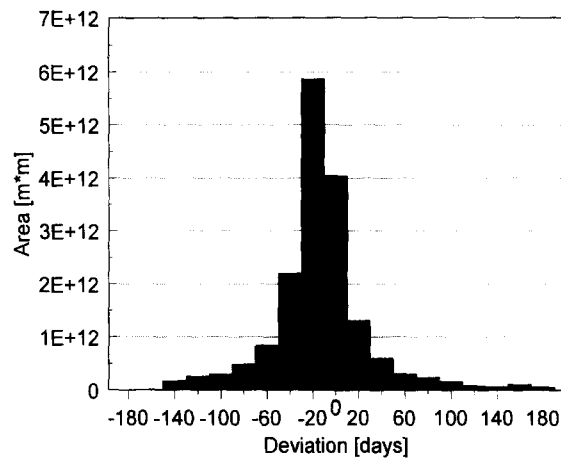


Fig. 7. Area-weighted frequency distribution of the deviation of the FBM-calculated *date of total leaf discoloration* from the respective NDVI-deduced date,  $t_3$ , for the vegetation types listed in Fig. 4a. Positive deviation values indicate that the FBM-calculated abscission date is earlier than the NDVI-deduced.

indicating that in the global mean the FBM predictions of leaf shooting lag only less than one week behind satellite detections. A 75% fraction of the area considered here shows predicted shooting dates lying within a range of  $\pm 30$  days compared to the satellite deduced dates. The distribution has its maximum at a difference of 0 days (i.e. the FBM exactly fits the NDVI deduced shooting day for the respective areas) and a standard deviation or mean quadratic error of  $\sigma = 34$  days. It should be noted that the difference in the time discretization of the NDVI-deduced shooting day (months) and the FBM-predicted shooting day (days) would produce a value of  $\sigma = 9$  days even under the assumption that the predicted shooting days would be exact. Considering this fact the width of the computed distribution is quite satisfactory for a global scale model which was *not* tuned to fit phenological data.

To test the FBM-calculated leaf abscission dates we compared the calculated date of total leaf discoloration with the satellite deduced  $t_3$ -values and display the result in Fig. 7 as done for the leaf shooting. We obtained a slightly broader, approximately Gaussian distribution with a mean difference value of  $-14$  days (i.e. the FBM calculated total discoloration is about two weeks too late) and a standard deviation of  $\sigma = 42$  days. The reason for this less accurate result is that the end of the vegetation period is mostly a continuous transition ending in total discoloration of the leaves of some species and can therefore hardly be detected exactly by evaluating NDVI signals. This is in contrast to the rather abrupt start of the vegetation period by leaf shooting which can be detected with higher accuracy providing therefore a more adequate phenology verification.

#### 4. Discussion

After developing a reliable algorithm for the detection of the large scale phenology of areas mainly covered by deciduous vegetation a useful tool for the validation of global seasonal vegetation models is now available. In the current study, the algorithm is applied to validate an equilibrium run of the prognostic FBM driven by a climatology representing a mean seasonality of the driving variables. Therefore the FBM predicts a mean phenology. In view of this fact we have used an average of the shooting and abscission dates as deduced from the NDVI time courses of three different years for the comparison with the FBM results.

Since the FBM structure allows also for transient calculations, a comparison with the predicted annual variability of shooting and abscission dates would be useful. Respective FBM runs driven by real climate time

courses of the 1980s are under way and will enable such a comparison to be made in the near future. The relatively coarse time resolution of the NDVI time series does not allow the detection of small interannual variations in phenology (e.g. in the temperate forests). Even the use of NDVI courses with higher time resolution (e.g. biweekly values) would not overcome this constraint for the reason that increasing noisyness of the data would decrease the reliability of the phenology deduced. On the other hand interesting results with respect to drought deciduous vegetation types are to be expected.

From the results presented in this study some major conclusions with respect to the FBM performance in different vegetation types can be drawn.

Firstly, the comparison of the satellite-derived shooting dates with those obtained from ground observations in temperate deciduous forest ecosystems showed that the first leaf emergence of the herbaceous layer was detected by the satellite and not the shooting dates of the dominant woody species. Using the ground phenology observations of temperate forest ecosystems it was possible to calibrate the proposed NDVI evaluation algorithm in order to detect the shooting date of the woody species. The FBM does not take into account the herbaceous layer in these ecosystems due to their relatively small contribution to the total carbon exchange fluxes which are mainly caused by the dominant woody species. Therefore it is appropriate to compare the FBM-predicted phenology for these ecosystems with the results of the calibrated NDVI evaluation algorithm. We could show that the simulated shooting times for the temperate deciduous forests reproduce the calibrated satellite observations very well (see Figs. 3 and 4).

However, for vegetation types where herbaceous and woody species play a more equal role with respect to the CO<sub>2</sub> exchange fluxes (e.g. savannas) one should expect that the FBM correctly predicts the first greening. Here the results of the comparison are slightly worse (they are responsible for the relatively flat left slope of the error distribution in Fig. 6). This is due to the integration of different plant functional types of one ecosystem into the simple compartment structure of the FBM (see Appendix A) and points to the necessity to improve the FBM structure by subdivision into the dominant functional types within one grid element.

It could be shown that in general the global phenology predictions of the FBM reproduce the NDVI-derived global patterns with a mean quadratic error of about one month, which is a reasonable result with respect to the remaining uncertainties in the NDVI evaluation. Nevertheless we expect a further decrease of this error after FBM improvements as mentioned above (the optimum result would be an error of 9 days due to discretization errors).

We consider the results of the presented study as a strong hint that the carbon flux balance criterion which is the main assumption underlying the FBM phenology modeling is at least a reasonable approximation for predicting the phenology of the different deciduous vegetation types on the global scale.

## Acknowledgements

This study was supported by the EU project ‘The Global Carbon Cycle and its Perturbation by Man and Climate II’, contract EV5V-CT-92-0119. We thank Franz-W. Badeck for helpful discussions, Jürgen Kindermann for thoroughly reading the manuscript and Gudrun Würth for providing the phenological data.

## Appendix A. Short description of the Frankfurt Biosphere Model

### A.1. Carbon allocation and phenology

As shown in Fig. 8 it is assumed that the assimilate production  $C_{ASS}$  is determined by the mass of compartment **GC**, reflecting the amount of leaves, the actual soil water content **SW** as well as by the external driving variables temperature  $T$  and irradiance  $I$ . This flux is to be partitioned according to present needs of the

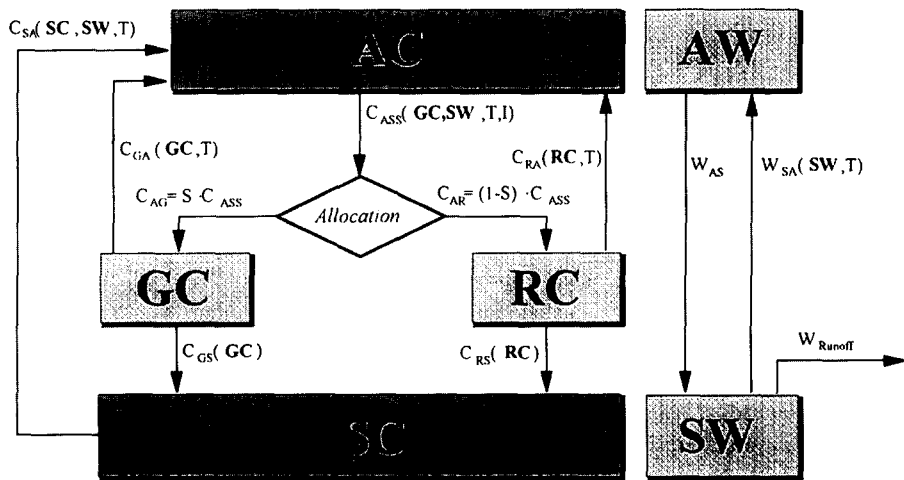


Fig. 8. Flow chart and model structure. Bold capital letters represent the reservoirs of C (second letter C) and water (second letter W): AC, atmospheric C; GC, C content of green biomass and feeder root biomass plus assimilate store; RC, C content of remaining biomass of biota ( $GC + RC = BC$ ); SC, C content of litter, humus and dead biomass; AW, water in the atmosphere; SW, soil water in the rooting zone. The capital letters C and W represent carbon and water fluxes. The indices indicate sources and sinks of these fluxes. The functional dependence of the fluxes on the driving variables and pool sizes is given in parentheses ( $T$ : hourly air temperature,  $I$ : hourly photosynthetic active radiation, PAR).  $W_{AS}$  is the daily precipitation,  $W_{SA}$  is daily actual evapotranspiration. The factor  $S$  represents the fraction of total assimilation  $C_{ASS}$  that is allocated to GC.

plant organs, namely the build-up and maintenance of the photosynthesizing tissue and of the feeder roots (represented by GC) on the one hand, and the build-up and maintenance of stems, branches and coarse roots (represented by RC) on the other. Furthermore, assimilates have to be translocated in order to fill particular storage organs, which are included in the C mass of the GC compartment as well.

The partitioning of the C assimilation flux  $C_{ASS}$  into the GC and RC compartment is derived in its seasonal and long-term patterns from two basic assumptions:

- The vegetation tends to maximize the amount of photosynthesizing tissue (contained in the GC compartment).
- It is possible to identify a function  $RC = \Omega(GC) = \xi \cdot GC^k$  determining the minimum amount of RC needed to support and maintain the given amount of GC.

We distinguish four different phenophases:

1. Shooting phase: the C gain from photosynthesis is greater than the C loss. The system allocates most of the assimilates to the GC compartment until the trajectory reaches  $\Omega(GC)$ , maximizing its production ability.
2. Secondary growth: the system is forced to allocate simultaneously into the GC and RC compartment according to the  $\Omega(GC)$  function.
3. Leaf shedding: at the end of the vegetation period, when unfavorable weather conditions do not allow biomass increase (e.g. drought, cold), a leaf abscission phase reduces the GC compartment to a remaining amount of feeder roots and assimilate store, which is proportional to the annual maximum of GC and characterized by the function  $RC = \Theta(GC) = \nu \cdot GC^k$ .
4. Dormancy phase: when the trajectory reaches the  $\Theta(GC)$  curve the dormancy phase starts. During this phase the biomass losses, as defined by the RC respiration and the total litter production  $C_{BH}$ , are distributed among the compartments so that the systems trajectory follows the  $\Theta(GC)$  curve. This phase ceases when the weather conditions allow a net biomass increase, assuming a total conversion of stored assimilates into leaf biomass and feeder roots.

## A.2. Calculation of fluxes

The net uptake of  $\text{CO}_2$  by plants is determined by a balance of two processes: C assimilation,  $C_{\text{ASS}}$  (i.e. the gross photosynthetic C fixation) and autotrophic respiration,  $C_{\text{GA}}$  and  $C_{\text{RA}}$ . As assimilation and respiration show different seasonal courses and different temperature responses, we think it is more convenient to model these processes separately instead of simulating the NPP directly.

## A.3. Uptake of $\text{CO}_2$

The effective C assimilation rate,  $C_{\text{ASS}}$ , can be considered as a product function of a term dependent on light and canopy structure, a temperature-dependent term and a soil water-dependent term. The dependence on irradiance and leaf area index, LAI, which is correlated with the **GC** compartment is modeled taking into account the light attenuation in the canopy. For the temperature dependence an optimum curve is used characterized by the minimum, maximum, and optimum temperature of photosynthesis. The dependence of photosynthesis on water availability, represented by the soil water content **SW**, is assumed to follow a saturation curve which is zero at the permanent wilting point and approaches one for field capacity.

## A.4. Release of $\text{CO}_2$ – autotrophic respiration

Autotrophic respiration,  $C_{\text{GA}}$  and  $C_{\text{RA}}$  respectively, is modeled similarly for both compartments, **GC** and **RC**, depending on the compartment size and an exponential function of the temperature corresponding to a constant  $Q_{10}$  value for each ecosystem type.

## A.5. Litter production

The litter production,  $C_{\text{GS}}$  and  $C_{\text{RS}}$ , is assumed to be proportional to the respective compartment size. For the **GC** compartment of the deciduous vegetation types an additional constant rate litter production occurs during the abscission phase.

## A.6. Release of $\text{CO}_2$ – heterotrophic respiration

For the climate response of the decomposition of dead organic matter,  $C_{\text{SA}}$ , we extended the model of Fung taking into consideration a linear dependence on compartment size and introducing a soil moisture factor analogous to the moisture dependence of photosynthesis.

## A.7. Water fluxes

Due to the close relation between assimilation and transpiration, the actual evapotranspiration,  $W_{\text{SA}}$ , is calculated by the product of potential evapotranspiration after Thornthwaite,  $W_{\text{PET}}$ , and the soil water-dependent function as used in the calculation of assimilation.

$W_{\text{Runoff}}$  comprises both surface runoff and drainage. It is taken as the surplus water when the soil water content reaches field capacity.

## A.8. Equilibrium model run

The model described above was run on a  $0.5^\circ \times 0.5^\circ$  grid until equilibrium (a stable limit cycle) was reached. As driving variables we used the climatology of Leemans and Cramer (1991) which contains typical annual courses of temperature, precipitation and cloudiness.

## Appendix B. The three-spline fit

For the approximation of a given NDVI-course we introduced the piecewise defined continuous function  $S(t)$ :

$$S(t) = \begin{cases} (N_2 - N_1) \cdot \frac{t - t_1}{t_2 - t_1} + N_1 & t_1 \leq t < t_2 \text{ (phase A)} \\ \frac{N_2 - N_1}{2t_2t_3 - t_2^2 - t_3^2} \cdot (t^2 - 2t_2t + t_2^2) + N_2 & t_2 \leq t < t_3 \text{ (phase B)} \\ N_1 & \text{otherwise (phase C)} \end{cases} \quad (3)$$

which is determined by the starting and end points of the tree splines:  $(t_1, N_1)$ ,  $(t_2, N_2)$  and  $(t_3, N_1)$  and therefore depending on five parameters. For the location of these points and the qualitative course of  $S(t)$  see Fig. 2a.  $S(t)$  is not a smooth function ( $S(t)$  is not differentiable at the starting and end points of the tree splines) because it is developed to sharply detect times of transitions which would not be possible with e.g. a Fourier approach.

We then minimized the mean absolute error,  $\sum_j |\text{NDVI}(T_j) - S(T_j)|$ , over all data points of a given NDVI( $T$ )-course by varying the five free parameters  $\{t_1, t_2, t_3, N_1, N_2\}$  under the restrictions  $t_1 < t_2 < t_3$  and  $N_1 < N_2$ . These restrictions guarantee even for noisy NDVI time series a qualitative  $S(t)$ -course which is interpretable in terms of leaf phenology.

To numerically solve this minimization problem we defined a grid in the  $(t, S)$ -plane and determined the optimal parameters using a simple numerical search algorithm which ensures the determination of the absolute minimum on this grid. For the  $t$ -axis we applied time steps as given by the NDVI data used, while the  $S$ -range from  $\min(\text{NDVI}(T))$  to  $\max(\text{NDVI}(T))$  was divided into  $n$  steps. A sensitivity analysis yielded that the resulting optimal  $\{t_1, t_2, t_3\}$ -set and the corresponding mean absolute error was rather insensitive against  $n$  for  $n \geq 4$ .

## Appendix C. Distortion of NDVI courses by the influence of snow water

In Fig. 9 we present the NDVI courses of tundra grid elements along a north/south transect. Fig. 9a shows the strong seasonal influence of the (melting) snow cover on the total NDVI signal which in the case of only sparse vegetation cover may lead to an inverse time course with its minimum during the vegetation period, due to the reflectances of persistent snow water. In Fig. 9b the vegetation signal overcompensates the negative background signal during the vegetation period. Negative NDVI values in spring indicate, however, a time course which is not mainly governed by the vegetation and thus unreliable for detecting the phenology. As can easily be seen in the southernmost grid element (Fig. 9c) even in NDVI courses being positive throughout the year a clear minimum may occur before the period of NDVI increase. Thus we agree with Box et al. (1989) who stated that monthly NDVI values in high latitudes are less reliable, especially in springtime. From this follows that in regions with frequently appearing type (Fig. 9b) grid elements the probability of the occurrence of type (Fig. 9c) time courses is high, too. We considered this relation by omitting from our evaluation those vegetation types, which show negative NDVI values in more than half the area actually covered with the respective vegetation type.

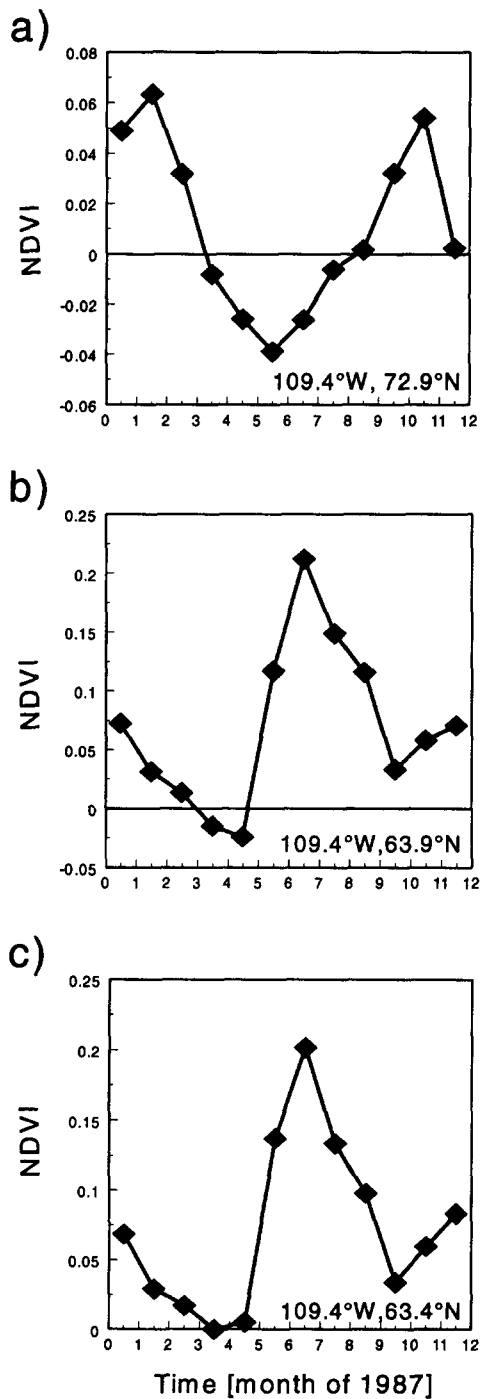


Fig. 9. Three NDVI courses (1987) of tundra grid elements along a north/south transect.

## Appendix D. Abbreviations

DD FST	Tropical/subtropical drought deciduous forest
CD FST 1	Cold deciduous forest, with evergreens
CD FST 2	Cold deciduous forest, without evergreens
XE FST	Xeromorphic forest/woodland
DD WDL	Tropical/subtropical drought deciduous woodland
CD WDL	Cold deciduous woodland
DD SHL	Drought deciduous shrubland/thicket
CD SHL	Cold deciduous subalpine/subpolar shrubland, dwarf shrubland
TUNDRA	Arctic/alpine tundra, mossy bog
TE GRL/WDL C3	Temperate grassland with woody tree cover (C3)
TE GRL/STP C3	Temperate grassland/steppe, prairie (C3)
TE GRL/STP C4	Temperate grassland/steppe, prairie (C4)
TE GRL/WDL C4	Temperate grassland with woody tree cover (C4)
TE SHL 1	Temperate dwarf shrubland (Eurasia)
TE SHL 2	Temperate dwarf shrubland (South America)
TR GRL/SAV	Tropical grassland/dry savanna
TR GRL/WDL	Tropical grassland/small-leaved thorn-tree woodland

## References

- Ackerman, T.L. and Bamberg, S.A., 1974. Phenological studies in the Mojave Desert at Rock Valley (Nevada Test Site). In: H. Lieth (Editor), *Phenology and Seasonality Modeling*. Springer, Berlin, pp. 215–226.
- Box, E.O., Holben, B.N. and Kalb, V., 1989. Accuracy of the AVHRR vegetation index as a predictor of biomass, primary productivity and net CO<sub>2</sub> flux. *Vegetatio*, 80: 71–89.
- Ellenberg, H., 1982. *Vegetation Mitteleuropas mit den Alpen in ökologischer Sicht*. Eugen Ulmer, Stuttgart.
- Janecek, A., Benderoth, G., Lüdeke, M.K.B., Kindermann, J. and Kohlmaier, G.H., 1989. Model of the seasonal and perennial carbon dynamics in deciduous-type forests controlled by climatic variables. *Ecol. Model.*, 49: 101–124.
- Kindermann, J., Lüdeke, M.K.B., Badeck, F.-W., Otto, R.D., Klaudius, A., Häger, Ch., Würth, G., Lang, T., Dönges, S., Habermehl, S. and Kohlmaier, G.H., 1993. Structure of a global carbon exchange model for the terrestrial biosphere: the Frankfurt Biosphere Model (FBM). *Water Air Soil Pollut.*, 70: 675–684.
- Kramer, K., 1994. A modelling analysis of the effects of climatic warming on the probability of spring frost damage to tree species in the Netherlands and Germany. *Plant Cell Environ.*, 17: 367–377.
- Leemans, R. and Cramer, W.P., 1991. The IIASA Database for Mean Monthly Values of Temperature, Precipitation, and Cloudiness on a Global Terrestrial Grid. RR-91-18, IIASA, Laxenburg, Austria.
- Lüdeke, M.K.B., Janecek, A. and Kohlmaier, G.H., 1991. Modelling the seasonal CO<sub>2</sub> uptake by land vegetation using the global vegetation index. *Tellus*, 43B: 188–196.
- Lüdeke, M.K.B., Badeck, F.-W., Otto, R.D., Häger, C., Dönges, S., Kindermann, J., Würth, G., Lang, T., Jäkel, U., Klaudius, A., Ramge, P., Habermehl, S. and Kohlmaier, G.H., 1994. The Frankfurt Biosphere Model. A global process oriented model for the seasonal and longterm CO<sub>2</sub> exchange between terrestrial ecosystems and the atmosphere. Part 1: Model description and illustrating results for the vegetation types cold deciduous and boreal forests. *Climate Res.*, 4: 143–166.
- Lüdeke, M.K.B., Dönges, S., Otto, R.D., Kindermann, J., Badeck, F.-W., Ramge, P., Jäkel, U. and Kohlmaier, G.H., 1995. Responses in NPP and carbon stores of the northern biomes to a CO<sub>2</sub>-induced climatic change, as evaluated by the Frankfurt Biosphere Model (FBM). *Tellus*, 47B: 191–205.
- Malaisse, F.P., 1974. Phenology of the Zambezi woodland area with emphasis on the Miombo ecosystem. In: H. Lieth (Editor), *Phenology and Seasonality Modeling*. Springer, Berlin, pp. 269–286.
- Matthews, E., 1983. Global vegetation and land use data base for climate studies. *Bull. Am. Meteorol. Soc.*, 64: 793–794.
- NGDC, 1992. Monthly generalized global vegetation index from NESDIS NOAA-9 weekly GVI data (Apr. 1985–Dec. 1988). Digital raster data on a 10-minute geographic (lat/long) 1080×2160 grid. In: *Global Ecosystems Database Version 1.0: Disc A*. NOAA National Geophysical Data Center, Boulder, CO.
- Olivares, E. and Medina, E., 1992. Water and nutrient relations of woody perennials from tropical dry forests. *J. Veg. Sci.*, 3: 383–392.

- Olson, J. and Watts, J.A., 1982. Major World Ecosystem Complexes Ranked by Carbon in Live Vegetation (Map). NDP-017, Oak Ridge National Laboratory, Oak Ridge, TN.
- Raich, J.W., Rastetter, E.B., Melillo, J.M., Kicklighter, D.W., Steudler, P.A., Peterson, B.J., Grace, A.L., Moore III, B. and Vörösmarty, C.J., 1991. Potential net primary productivity in South America: application of a global model. *Ecol. Appl.*, 1: 399–429.
- Ruimy, A., Dedieu, G. and Saugier, B., 1991. Estimation de la productivité primaire nette continentale a partir de mesures satellitaires. *Atelier de Modélisation de l'Atmosphère*, 26–27 November 1991. CNRMm, Toulouse, 10 pp.
- Schnelle, F., 1985. 25 Jahre phänologische Beobachtungen in den internationalen phänologischen Gärten. *Arbor. Phaenol.*, 29: 1–44.
- Schwartz, M.D. and Marotz, G.A., 1986. An approach to examining regional atmosphere–plant interactions with phenological data. *J. Biogeogr.*, 13: 551–560.
- Sellers, P.J., Berry, J.A., Collatz, G.J., Field, C.B. and Hall, F.G., 1992. Canopy reflectance, photosynthesis and transpiration. III. A reanalysis using improved leaf models and a new canopy integration scheme. *Remote Sens. Environ.*, 42: 187–216.
- Tucker, C.J. and Sellers, P.J., 1986. Satellite remote sensing of primary production. *Int. J. Remote Sens.*, 7: 1395–1416.
- Tucker, C.J., Townshend, J.R.G. and Goff, T.E., 1985. African land-cover classification using satellite data. *Science*, 227(4685): 369–375.
- Walter, H., 1968. Die Vegetation der Erde. In *Öko-Physiologischer Betrachtung. Die Gemäßigten und Arktischen Zonen*. Vol. 2. Gustav Fischer, Stuttgart.